Impact of the Temperature on the Interactions Between Common Variants of the SARS-CoV-2 Receptor Binding Domain and the Human ACE2

Catherine Forest-Nault
Polytechnique Montreal
Izel Koyuturk
National Research Council of Canada
Jimmy Gaudreault
Polytechnique Montreal
Alex Pelletier
National Research Council of Canada
Denis L'Abbé
National Research Council of Canada
Brian Cass
National Research Council of Canada
Louis Bisson
National Research Council of Canada
Alina Burlacu
National Research Council of Canada
Laurence Delafosse
National Research Council of Canada
Matthew Stuible
National Research Council of Canada
Olivier Henry
Polytechnique Montreal
Gregory Crescenzo (gregory.decrescenzo@polymtl.ca)
Polytechnique Montreal
Yves Durocher
National Research Council of Canada

Article

Keywords:

Posted Date: May 11th, 2022

DOI: https://doi.org/10.21203/rs.3.rs-1585804/v1

Abstract

Several key mutations in the Spike protein receptor binding domain (RBD) have been identified to influence its affinity for the human Angiotensin-Converting Enzyme 2 (ACE2). Here, we perform a comparative study of the ACE2 binding to the wild type (Wuhan) RBD and some of its variants: Alpha B.1.1.7, Beta B.1.351, Delta B.1.617.2, Kappa B.1.617.1, B.1.1.7+L452R and Omicron B.1.1.529. Using a coiled-coil mediated tethering approach of ACE2 in a novel surface plasmon resonance (SPR)-based assay, we measured interactions at different temperatures. Binding experiments at 10°C enhanced the kinetic dissimilarities between the RBD variants and allowed a proper fit to a Langmuir 1:1 model with high accuracy and reproducibility. The Omicron RBD variant has the highest affinity for ACE2, followed by the Alpha (N501Y) and Beta (K417N, E484K, N501Y) variants. However, variants with the L452R mutation, i.e. the B.1.1.7+L452R (L452R, N501Y; which we called AlphaP), Delta (L452R, T478K) and Kappa (L452R, E484Q) showed faster kinetics resulting in significatively lower affinities compared to the other variants. Our study emphasizes the importance of SPR-based assay parameters in the acquisition of quality data and offers a powerful tool to deepen our understanding of the role of the various RBD mutations in ACE2 interaction binding parameters.

Introduction

The ongoing spread of the coronavirus disease 2019 (COVID-19) caused by severe acute respiratory syndrome coronavirus 2 (SARS-CoV-2) continues to lead to the emergence of new variants and epidemic waves. Several SARS-CoV-2 lineages are defined as variants of concerns (VOCs) by the World Health Organization (WHO), including the B.1.1.7 (Alpha), the B.1.351 (Beta), the B.1.617.2 (Delta) and the B.1.1.529 (Omicron), while the variants B.1.617.1 (Kappa) and B.1.1.7 + L452R (named herein AlphaP) are defined as variants of interest (VOIs) [1]. These variants present key mutations within their spike protein and more specifically in its receptor binding domain (RBD). The RBD interacts directly with the human angiotensin-converting enzyme 2 (ACE2), which is expressed at the cell surface of many cell types and initiates the virus cell entry process [2]. Intensive efforts have thus focused on understanding the binding mechanism of the RBD region to ACE2 [3–7]. While these studies have provided key information, affinity and kinetic estimates of the RBD / ACE2 interaction that were reported vary by 10 to 20 folds from one study to the other [3,7–12]. Part of the differences can be attributed to the design of the reported (SPR-based) assays where the surface-immobilized protein, the immobilization strategy and the experimental temperature can greatly influence the derived apparent kinetic and thermodynamic parameters [13,14].

We here report the development of an optimized SPR-based assay for the kinetic analysis of the interaction between the RBD of seven common variants (Wild type, Alpha, AlphaP, Beta, Delta, Kappa and Omicron) and ACE2. A capture strategy based on coiled-coil interactions enabled us to reduce common artifacts and record interaction data that were accurately fitted with a Langmuir 1:1 kinetic model to identify the apparent kinetic constants k_{on} and k_{off} for each RBD / ACE2 interaction. By modulating the temperature at 10°C, 25°C and 37°C, we were able to unravel the differences between the kinetic profiles

of the RBD / ACE2 interaction for each variant. Our results, in agreement with others, point out that the RBD mutation with the biggest impact on the RBD / ACE2 interaction is the N501Y. The Alpha variant that only harbors the N501Y mutation has a ~ 15-fold higher affinity (0.18 nM) than the wild type RBD when measured at 10°C [3,7,15–17]. The Beta variant harboring mutations N501Y, E484K and K417N has only a ~ 5-fold affinity increase, more likely due to the K417N mutation already reported to lead to a decreased affinity in several studies. The Delta, Kappa and AlphaP all present the L452R mutation and exhibit lower affinity by ~ 40, 10 and 5-fold, respectively. Of interest, the Kappa and AlphaP standard entropy changes, as derived from a Van't Hoff plot analysis, were of the opposite sign compared to the other variants. Finally, we found that the Omicron variant, the one with the highest number of mutations in its RBD region (15 mutations), has the highest affinity for ACE2 with a K_D of 0.14 nM at 10°C.

Results

The goal of this study was to develop an optimized SPR-based assay to analyze the interactions between the RBD of important variants with ACE2. For assay validation, we chose the variants of concerns (VOCs) Alpha, Beta, Delta and Omicron as well as two former variants of interest (VOIs) Kappa and AlphaP. All the mutants were compared to the original strain identified in Wuhan, China and referred here as wild type. Table 1 summarizes the mutations in the RBD domain of the variants included in this study.

Table 1
RBD variants and their mutations from the original strain (Wuhan)

Wild type (Wuhan)	Alpha B.1.1.7	AlphaP B.1.1.7 + L452R	Beta B.1.351	Delta B.1.617.2	Kappa B.1.617.1	Omicron B.1.1.529
G339						D339
S371						L371
S373						P373
S375						F375
K417			N417			N417
N440						K440
G446						S446
L452		R452		R452	R452	
S477						N477
T478				K478		T478
E484			K484		Q484	A484
Q493						R493
G496						S496
Q498						R498
N501	Y501	Y501	Y501			Y501
Y505						H505

Our experimental approach relied on two distinct 5 heptad-long (i.e., 35 amino acid-long) non-natural coil peptides denoted E5 and K5 peptides. The E5 coil peptide (EVSALEK heptad) and the K5 coil peptide (KVSALKE heptad) are known to heterodimerize and form a very stable coiled-coil motif through hydrophobic and electrostatic interactions [18,19]. Our previous research work related to monoclonal antibodies binding to Fcγ receptor ectodomains has already demonstrated the various advantages of a coiled-coil based ligand capture approach for SPR-based assays in terms of simplicity, reproducibility, and stability over time [20]. Here, we covalently immobilized the K5 coil peptides onto the surface of the biosensor via a single engineered cysteine and produced the soluble monomeric ACE2 receptor with a C-terminal E5 coil tag (ACE2-E5) in mammalian cells (Fig. 1).

The E5 coil tag enabled a stable and oriented capture of ACE2 onto the K5 coil functionalized SPR surface. To limit SPR artifacts, we captured a consistently low amount of ACE2-E5 (~ 60 RUs) leading to

a constant maximal resonance signal (R_{max}) for all injected RBD variants of 16 ± 3 RUs and we performed every injection cycle at a flowrate of 50 µL/min. A regeneration step (6M guanidium chloride) promoting the dissociation of the coiled-coil complex was performed to enable the capture of fresh ACE2-E5 for each new cycle.

We performed all kinetic experiments at three different temperatures (10°C, 25°C and 37°C) and analyzed the recorded sets of sensorgrams with a 1:1 Langmuir interaction model (Fig. 2–3). We observed clear differences in the sensorgram profiles of the variants that do not contain the L452R mutation (Fig. 2) from the ones that do (Fig. 3). Our data highly suggest that the presence of the L452R mutation accelerates both association and dissociation with ACE2.

Figure 2 SPR sensorgrams recorded for the RBD variants that do not contain the L452R mutation interacting with tethered ACE2 at different temperatures. The sensorgrams corresponding to variant injections at 10, 25 and 37°C were globally fitted with a 1:1 Langmuir binding model (solid black lines). Residual plots are included underneath each sensorgram series.

For all variants at 10°C, we observed excellent fits of the experimental data with a simple kinetic model. We observed no obvious trend in the residual plots for most sensorgrams recorded at 10°C and χ^2 values in the order of 10^{-2} were calculated for all fits to a 1:1 kinetic model at this temperature, which is consequent with the level of measurement noise. Distinct curvatures and spikes were observed in the residual plots at the beginning of the association and dissociation phases for higher temperatures. The adequacy between the collected data and the Langmuir model also decreased as the assay temperature increased. This deviations from a simple behavior cannot be attributed to biases related to the coiled-coil mediated capture since, in the case of the Alpha and Omicron RBD mutants, a good adequation, χ^2 of 0.07 and 0.06 respectively, was still observed at 25°C.

The sensorgrams of the three variants with the L452R mutation were less in adequation with a 1:1 kinetic model, as one can judge from the quality of the fits and the residual plots or from the χ^2 values. The kinetic constants for the various interactions shown in Fig. 2 determined at 10°C and 25°C are given in Table 2.

Table 2
Kinetic constants of the interactions between the RBD variants and ACE2 at 10°C and 25°C. * Indicates kinetic constants for which fits were judged imperfect.

	10°C		25°C	
RBD Variants	k_{on} (10^5 M^{-1} s^{-1})	k_{off} (10^{-4} s^{-1})	k_{on} (10^5 M^{-1} s^{-1})	k_{off} (10^{-4} s^{-1})
Wild type	1.76 ± 0.29	4.45 ± 0.32	8.02 ± 1.10	52.80 ± 5.50
Alpha	4.34 ± 0.50	0.79 ± 0.08	11.10 ± 1.53	6.43 ± 1.14
AlphaP	9.46 ± 4.20*	76.7 ± 30.1*	-	-
Beta	3.92 ± 0.41	2.13 ± 0.14	11.39 ± 1.24	16.61 ± 2.74
Delta	4.21 ± 0.31*	447 ± 88*	-	-
Kappa	1.89 ± 0.98*	52.8 ± 18.3*	-	-
Omicron	4.24 ± 0.02	0.57 ± 0.02	17.90 ± 3.59	6.92 ± 0.39

The apparent kinetic constants for the AlphaP and Kappa variants are provided for an indicative comparison to the other mutants. However, for these variants, the fits to the 1:1 kinetic model are poor. Thus, the derived kinetic constants must rather be regarded as indicative order of magnitudes. The sensorgrams of the AlphaP and Kappa variants at 25°C were only analyzed and validated by a steady-state model.

Equilibrium constants (K_D) were then calculated by computing the ratio of the kinetic constants (k_{off}/k_{on}) when the simple kinetic model adequately depicted the experimental data. For all other cases, K_D was calculated by a steady-state model using the pseudo-equilibrium responses reached at the end of the RBD injections. The standard entropy and standard enthalpy changes were then estimated by a Van't Hoff analysis (Table 3).

Table 3
Thermodynamic evaluation of the interaction of RBD variants with ACE2. * Indicates kinetic constants that were calculated using a steady-state model.

	10°C - K_D (nM)	25°C - K_D (nM)	37°C - K_D (nM)	ΔG° (kcal mol^{-1})	ΔH° (kcal mol^{-1})	ΔS° (cal K^{-1} mol^{-1})
Wild type	2.56 ± 0,35	6.73 ± 0.03	19.14 ± 1.60	-10.99	-12.67	-5.97
Alpha	0.18 ± 0.03	0.64 ± 0.20	2.70 ± 0.40	-12.43	-17.45	-16.97
AlphaP	11.84 ± 6.29	15.61 ± 0.67	22.98 ± 1.56*	-10.52	-4.06	21.27
Beta	0.55 ± 0.06	1.48 ± 0.40	5.92 ± 1.33	-11.71	-15.30	-11.95
Delta	106 ± 17	198 ± 48	595 ± 29*	-9.00	-10.91	-6.21
Kappa	29.47 ± 5.58	69.02 ± 4.86	75.5 ± 11.51*	-9.56	-9.56	0.48
Omicron	0.14 ± 0.01	0.40 ± 0.07	1.98 ± 0.17	-12.43	-16.97	-14.58

A Van't Hoff plot was constructed for each RBD variant and showed good fits with R^2 coefficients greater than 0.94 in all cases except the Kappa variant (R^2 of 0.88) (Supplementary Information Figure S1), thus validating the inherent hypothesis of temperature independence for ΔH° and ΔS° of this system.

Finally, we extended our assay to the evaluation of binding kinetics between various glycoforms of ACE2-E5 with SARS-CoV-2 RBD wild type. Seven glycoforms of ACE2-E5 harboring or not α2,3 sialylation, α2,6 sialylation or fucosylation were produced using glycoengineered Chinese Hamster Ovary (CHO) cells. The thermodynamic constants of these ACE2 glycoforms at 10°C are presented in Table 4.

Table 4
Affinities of various ACE2 glycoforms for wild type RBD. + and - signs indicates the presence or absence of the glycosylation type.

	K_D (nM)	k_{on} (10^5 M^{-1} s^{-1})	k_{off} (10^{-4} s^{-1})	Glycoform
WT	2.57 ± 0.09	1.76 ± 0.05	4.55 ± 0.04	+ α2,3 sialylation - α2,6 sialylation + Fucosylation
WT/ST6	2.61 ± 0.12	1.68 ± 0.12	4.38 ± 0.11	+ α2,3 sialylation + α2,6 sialylation + Fucosylation
F15	3.68 ± 0.11	1.30 ± 0.02	4.79 ± 0.10	+ α2,3 sialylation - α2,6 sialylation - Fucosylation
dKO2	2.96 ± 0.01	1.58 ± 0.01	4.66 ± 0.02	- α2,3 sialylation - α2,6 sialylation - Fucosylation
dKO2/ST6	3.47 ± 0.07	1.39 ± 0.05	4.81 ± 0.03	- α2,3 sialylation + α2,6 sialylation - Fucosylation
S9	2.35 ± 0.12	1.94 ± 0.02	4.55 ± 0.27	- α2,3 sialylation - α2,6 sialylation + Fucosylation

The different ACE2 glycoforms were produced in glycoengineered cell lines with knockout genes as previously reported [21]. While F15 and S9 cell lines produce glycoproteins without core-fucose sugar and α-2,3-linked sialic acid, respectively, dKO2 is a double knock-out cell line lacking both core-fucosylation and α-2,3 sialylation. The cell lines WT/ST6 and dKO2/ST6 express stably the human *ST6Gal1* gene and are thus capable of generating glycans with terminal α2,6 sialylation. At 10°C, no statistical differences were observed between the thermodynamic (Table 4) and kinetic constants depicting the interactions of the various ACE2 glycovariants with the wild type RBD.

Discussion

As part of the global effort towards a better understanding of the infection mechanisms of SARS-CoV-2, we have reported here a surface plasmon resonance (SPR)-based approach allowing for the kinetic evaluation of ACE2 binding to various SARS-CoV-2 RBDs. Our experimental approach allowed us to depict the data with a 1:1 Langmuir kinetic model and thus draw reliable and meaningful conclusions about the impact of key RBD mutations. Several studies have already employed SPR biosensing to analyze the interaction of SARS-CoV-2 variants to ACE2, but different experimental approaches resulted in a wide range of thermodynamic and kinetic constants (K_D varying from 4 to 80 nM) that are difficult to compare from one study to the other [3,7–12]. In fact, the choice of the ligand (proteins captured at the biosensor surface), the capture strategy, the ligand density, the flowrate, and the experimental temperature all may affect the recorded data and thus bias the interpretation [22]. The experimental conditions must be optimized to minimize potential artifacts such as mass transport limitations, avidity, steric hindrance, and rebinding [23].

In this endeavor, our strategy was to focus only on the RBD region instead of using the complete spike protein ectodomain since its trimeric nature may introduce potential artifacts in the kinetic analysis [12,24]. The spike protein is a large trimeric glycoprotein (~ 550 kDa) bearing three RBDs all capable to interact with an ACE2 receptor. This complex, spike / ACE2, is thus prone to avidity and rebinding artifacts in SPR-based assays. Moreover, it has been shown that each RBD can individually be either in an up or down conformation which influence the overall spike affinity for ACE2 and add a heterogeneity bias in the analytes of the SPR-based assay [23]. The proportion of RBD in each conformation can vary for different variants leading to even more complexity in the analysis of the spike / ACE2 interaction [24,25]. Conducting SPR-based assay with the RBD as the analyte limits these biases and simplify the kinetic profiles of the data collected, as the RBD / ACE2 follows, in theory, a 1:1 binding model as we were able to observe at 10°C. It is then easier to obtain good quality and robust data to better understand the subtle affinity differences between SARS-CoV-2 variants and the ACE2 receptor.

Also, we chose to use ACE2 as the ligand, to better mimic the biological course of action where the virus interacts with ACE2 exposed at the surface of human cells. We optimized our SPR-based assay by tethering ACE2 onto the biosensor surface in a highly stable and oriented manner. Our coiled-coil mediated strategy allowed us to capture a constant low density of fresh ACE2-E5 at the surface for each experimental cycle; a low density of ligands on the surface reduces the risk of mass transport limitations and rebinding artefacts, which affect the kinetic interpretation of the data [26,27].

The immobilization strategy is also a determinant factor in SPR for stable and reproducible results. Studies relying on an amine covalent coupling approach are subject to heterogeneous immobilized ligand orientations and progressive loss of bioactivity over time and regeneration steps, which can translate into more complex kinetics and variable results [28]. The oriented immobilization of the ligand by a capture agent (such as the coiled-coil peptide system) enables more control and flexibility over the density of ligand on the surface and guaranties the structural integrity of the ligand [23,29]. Our coiled-coil approach proved to be simple and highly reproducible as we were able to obtain robust and reproducible results

over five different sensor chips. The wild type (n = 5) and Alpha variants (n = 6) were our controls for every new sensor chip and showed minimal standard deviations on the calculated constant of affinity K_D at 10°C (2.56 ± 0.35 nM for wild type and 0.18 ± 0.03 nM for Alpha).

We also varied the experimental temperature and underlined the importance of this parameter on the measurements of simple kinetics for the RBD / ACE2 interactions. At 37°C, although this temperature is interesting to better understand / mimick the molecular interactions during infection, the interaction kinetics were fast and deviated from a 1:1 kinetic model. This complexity can be attributed to an enhanced mobility and conformation change of the RBD loop interacting with ACE2 at higher temperatures [24,30,31]. Other research groups performed their analysis at 25°C, which is the most common temperature in SPR-based assays [9,32]. We were able to obtain acceptable fits with a 1:1 Langmuir binding model at 25°C but slowing the kinetics at an even lower temperature, i.e. 10°C, enabled us to observe excellent fits and enhanced the differences between the variants, better highlighting the impact of RBD mutations on ACE2 binding. We report comparable association rate constants between the Alpha, Beta and Omicron variants resulting in ~ 2.5 to 3-time faster binding than the wild type RBD (k_{on} = 1.8 ± 0.3 $x10^5$ M^{-1}. s^{-1}, Table 2). The differences were more apparent in the dissociation rates where the Omicron and the Alpha presented the slowest rates at 0.57 ± 0.02 $x10^{-4}$ s^{-1} and 0.79 ± 0.08 $x10^{-4}$ s^{-1} respectively, which is 5 to 8 times slower than the wild type RBD. Meanwhile, the dissociation rate of the Beta variant is only 2 times slower. These kinetics confer the Omicron and the Alpha RBD variants with the highest affinities for ACE2, with ~ 20- and 15-fold decreases in K_D compared to the wild type RBD, respectively. Several studies have reported an increased affinity for the Alpha variant binding to ACE2 similar to our findings at 25°C (~ 10-fold), and 37°C (~ 7-fold) [3,11,17,32]. This increased affinity is linked to the only RBD mutation, N501Y [33,34]. In fact, Tian et al. demonstrated that the enhancement of the affinity of RBD / ACE2 interaction results from the ability of the RBD mutant tyrosine sidechain to perform π-stacking interactions with the Y41 sidechain of ACE2 [17].

The observed binding enhancement for the Omicron variant, however, is more complex to dissect due to the high number of mutations present at the interface with ACE2. Recent *in silico* models highly suggest that four key mutations contribute to this stronger interaction: S477N, G496S, Q498R and N501Y [35]. Other point mutations, such as H505Y and K417N, were observed to negatively impact the interactions with ACE2, which modulates the affinity to a similar level to that of the Alpha variant [36–38]. Further work is still needed to understand the individual and/or combine influence of Omicron mutations on its affinity for ACE2.

The effect of the K417N mutation is more predominant for the Beta RBD-ACE2 complex where this RBD variant expresses two additional mutations: E484K and N501Y. The positive effect of the N501Y mutation seems to be counteracted by the K417N mutation, resulting in only a 5-fold affinity enhancement compared to the wild type at 10°C (Fig. 3). In fact, the replacement of the lysine at position 417 by an asparagine disables the formation of a salt bridge between RBD K417 and ACE2 D30 in the wild type RBD / ACE2 complex [39]. The absence of this salt bridge translates to a decreased affinity as

observed in this work (Fig. 4) and in several other studies [7,32,40]. Our study shows that the E484K mutation has no significant impact on the binding affinity to ACE2, while other studies have reported conflicting results [9,35,41].

The AlphaP (L452R/N501Y), Delta (L452R/T478K) and Kappa (L452R/E484Q) variants all presented faster association and dissociation rates at all temperatures. They also exhibited a lower affinity for ACE2, i.e., 5-, 40- and 10-fold decreases respectively compared to the wild type, at 10°C. Based on these results, we could infer that the L452R mutation disturbs the binding to ACE2 and that, while it is compensated by the N501Y mutation in AlphaP, its effect is more apparent in Delta and Kappa. These results contrast with some studies that measured similar or slightly higher affinities for these variants compared to wild type [42,43]. However, the impact of L452R mutation on the RBD / ACE2 interaction is still debated as several studies demonstrated that it does not play a major role in the interaction with ACE2 [5,44,45]. In fact, some have suggested that the L452R mutation abrogates a hydrophobic patch formed by the amino acids L452, L492 and F490 [46]. The loss of this patch could impact stability of the RBD and possibly its complexation with ACE2, as suggested by our results. Moreover, L452 is not directly engaged with any ACE2 residue, which led research groups to focus on its impact on binding to antibodies instead of ACE2. A recent study showed that the L452R mutation enhances the viral replication by increasing the S protein stability and viral infectivity [47]. Moreover, the second mutation (E484Q) in the Kappa variant was also shown to weakly affect its interaction with ACE2. E484 only weakly interacts with ACE2 K31 and its substitution by a glutamine residue decreases binding [46]. Both mutations, L452R and E484Q are not involved in the interaction with ACE2, as shown for the other mutations, and most studies have linked them to an enhanced immune evasion from neutralizing antibodies [39,48–51]. However, the T478K mutation on Delta has been linked to a higher affinity for ACE2 due to the introduction of a positive charge on the lysine residue [52]. Some studies have shown, in the context of a trimeric spike construct, that the apparition of a positive electrostatic charge from T478K mutation stabilizes the RBD and favors its up conformation, leading to a better interaction with ACE2 [30,31,43].

Thermodynamic differences were also apparent in the enthalpic and entropic values measured by Van't Hoff plots for the AlphaP and Kappa. Enthalpic changes favor binding in all cases, as is inferred from a negative $\Delta H°$, indicative of an exothermic reaction. Amongst the variants that were studied, Alpha, Beta and Omicron showed the most exothermic behavior, whereas enthalpic contributions were the weakest for Kappa and AlphaP. Entropic contributions showed the opposite trend. They were shown to hamper binding to ACE2 for Alpha, Beta, Delta and Omicron (and wild type) whereas they contributed to the stability of the RBD / ACE2 complex for Kappa and AlphaP. The L452R mutation could be in part responsible for the opposite trends in enthalpic and entropic changes, as it is common to both Kappa and AlphaP. The L452R impact on Delta RBD / ACE2 thermodynamic values could be balanced by the T478K mutation which integrates a second positive charge and was shown to contribute to RBD conformation stabilization [31,49].

Our optimized SPR-based assay showed to be a robust approach to better reveal subtle changes in kinetic and thermodynamic data defining the interaction between the RBD of SARS-CoV-2 variants and human ACE2. We also took advantage of this assay to look at the impact of ACE2 glycosylation profiles upon RBD binding, as both ACE2 and RBD / spike are glycoproteins and it has been suggested that RBD and ACE2 glycans may contribute to binding stabilization [33,53,54]. At 10°C, we observed slight differences, i.e., less than 1.5-fold, between afucosylated ACE2 glycoforms, (F15, dKO2 and dKO2/ST6) and the WT ACE2 produced in CHO cells. To the best of our knowledge, no other studies observed an influence from fucosylation. Our results did not show a detectable influence from sialylation on the affinity between ACE2 and the wild type RBD. Other studies report a decreased affinity between sialylated ACE2 glycoforms with SARS-CoV-2 SPIKE protein [54–56]. Therefore, it would be interesting to further increase the sialylation level of ACE2 to see its impact using our enhanced SPR assay at low temperature. Moreover, the RBD region only harbor two N-glycosylation and up to 5 O-glycosylation sites [57] while the S1 domain of the spike protein contains 13 N-glycans. It may thus be of interest to adapt this SPR assay to the S1 domain.

In summary, we present an optimized SPR-based assay to enhance our understanding of the binding mechanisms between SARS-CoV-2 RBD and the human ACE2. The use of the K5/E5 coiled-coil tethering strategy resulted in a high reproducibility in our results while a low experimental temperature of 10°C enabled us to collect data depicted by a simple 1:1 Langmuir kinetic model. Altogether, this allowed us to precisely characterize the interactions of SARS-CoV-2 RBD variants with ACE2. This approach could be used to rapidly compare new variants of concern to those reported here and infer on their capacity to infect human cells.

Materials And Methods

Plasmids

The human ACE2 cDNA (UniProtKB-Q9BYF1) was synthesized by GenScript and optimized for expression in CHO cells. The construct encodes a human interleukin 10 signal peptide (MHSSALLCCLVLLTGVRA) followed by a Twin-Strep-tag II-$(His)_6$-FLAG tag on the N-terminus of the mature ACE2 receptor ectodomain (amino acids 20–613). An E5 coil sequence flanked by glycine linkers ($GGGG[EVSALEK]_5GGG$) was added in-frame at the ACE2 C-terminus. The cDNA was cloned into pTT5® expression using EcoRI and BamHI restriction enzymes.

Human beta-galactoside alpha-2,6-sialyltransferase 1 (*ST6Gal*1 or hST6) was also cloned into pTT® vector as described previously to modify the glycosylation of the ACE2 receptor [58].

The RBD sequences ($RBD^{319-541}$) of the SARS-CoV-2 spike protein (YP_009724390.1, Wuhan-Hu-1 strain or its variants) encodes a C-terminal $(His)_6$-FLAG tag and were cloned into the pTT5® vector using EcoRI and BamHI.

Protein expression and cell culture

Fut8 (F15), *ST4Gal4* (S9) as well as *Fut8* and *ST3Gal4* (dKO2) knock-out CHO cell lines were derived from CHO^{55E1} cells [59] using CRISPR/Cas9 as described elsewhere [21] and were used for transient ACE2 receptor expression following a previously reported protocol [60,61]. In brief, cells were maintained in a chemically-defined proprietary media formulation supplemented with 4 mM L-glutamine and incubated in shake flasks (Corning, NY, USA) under agitation (120 rpm) at 37°C, 5% CO_2. Two days prior to transfection, cells were seeded at 1×10^6 cells/mL in the same media to achieve a cell density of $\sim 8 \times 10^6$/mL on the day of transfection. Right before transfection, cells were diluted with 2 % fresh media and dimethylacetamide was added to 0.08 % (v/v). PEI-Max (Polysciences) was used to transfect cells at a DNA:PEI (polyethylenimine) ratio of 1:7 (w:w) and plasmid DNA final concentration was 1.4 µg/mL in cell culture media. The transfected DNA was a mix of 8 % (w/w) of the different pTT5-RBD constructs or pTT241-ACE2 ECD, 1 % pTT-Bcl-XL (anti-apoptotic effector) and % pTT-GFP. The hST6 expression vector was co-transfected with ACE2-ECD vector in dKO2 cells (dKO2/ST6) and WT CHO cells (WT/ST6). At 24h post-transfection, expression of the ACE2 was induced by adding 2 µg/mL of cumate and all cultures were supplemented with Anti-Clumping Supplement (1:500 dilution) (Irvine Scientific) as well as Feed 4 (2. % v/v) (Irvine Scientific) before moving to a 32°C incubator. At 5 days post-transfection, cultures were fed with additional 5% of Feed 4 and additional glucose was added every 2–3 days to maintain a minimal concentration of 17 mM. Cell supernatants were collected at 6–7 days post-transfection.

Protein purification

All constructs were purified essentially as previously described [57]. A first immobilized affinity chromatography (IMAC) step was performed using Nickel Sepharose Excel resin (GE Healthcare). Columns were equilibrated with equilibration buffer (50 mM $NaPO_4$ pH 7.8, 300 mM NaCl) and supernatants were loaded at 3mL/min. Columns were washed once with 50 mM $NaPO_4$ pH 7.8, containing 300 mM NaCl and 10 mM imidazole and eluted with the same buffer containing 300 mM imidazole. Wild type RBD and its variants were further purified using Superdex75 gel filtration column (GE Healthcare) except for the Omicron variant that was further purified by anti-FLAG chromatography [60] prior to Superdex75 gel filtration. This is necessary to separate monomers from dimers. The IMAC-purified ACE2 protein was loaded on Strep-Tactin XT Superflow high-capacity resin (IBA Lifesciences, Germany) according to the manufacturer's instructions. Buffer exchange was done with desalting columns (GE Healthcare) with PBS. Purified proteins were quantified using a NanoDrop Spectrophotometer (ThermoFisher). Finally, SDS-PAGE and total protein staining (Coomassie Blue) were performed using standard methods.

Surface Plasmon Resonance (SPR)

SPR experiments were performed using a Biacore T100 system (GE Healthcare) and research-grade CM5 sensor chips from Cytiva (Series S Sensor chip CM5, cat #29104988). The running buffer was HBS-EP+

(10mM HEPES, 0,15 M NaCl, 3mM ethylenediaminetetraacetic acid (EDTA), and 0,05% [v/v] surfactant P20, pH 7,4) from Cytiva as well (cat #BR100669).

Cysteine-tagged K5 peptides (CGG-$[KVSALKE]_5$) were synthesized by the peptide facility at University of Colorado, as previously described [62]. K5 peptides were covalently immobilized on the carboxymethyl-dextran sensor surface at about 1200 RUs on the reference and experiment flow cells as described by Murschel et al [18]. E5 coil tagged ACE2 receptors, diluted at 1 µg/mL, were captured on the experiment surface previously functionalized with the K5 peptide, via E5/K5 coiled-coil interactions at a flow rate of 10 µL/min. Approximately 60 RUs of ACE2 receptors were captured on the surface for all experimental cycles, for all RBD variants and temperatures. No ACE2 was injected over the reference surface. The surfaces were regenerated with three 15 s pulses of 6 M guanidium/HCl at 100 µL/min.

The Wild type, Alpha, Beta and Omicron RBD variants were injected for 460s over the captured ACE2 receptors and control surfaces at a flow rate of 50 µL/min at six concentrations between 0.5 nM and 100 nM in duplicate or triplicate. The dissociation was then monitored for 1250 s for Wild type, Alpha and Beta, and 1800 s for Omicron. As for the AlphaP and Kappa RBD variants, the injection was conducted between 80 and 200 s depending on the experimental temperature and the dissociation was monitored for at least 150 s. The experimental temperatures were 10°C, 25°C and 37°C. Each experiment was repeated at least 2 times and up to 6 times at 10°C. The data acquisition frequency was set to 10 Hz.

Sensorgrams were referenced by subtracting the signal recorded on the reference surface (with no ACE2) to that recorded on the active surface (with ACE2). Blank injections were also performed to subtract out the effects of buffer changes, temperature drifts and mechanical artifacts. This process is called double-referencing [13].

Data analysis

The interaction between the immobilized ACE2 and the injected RBD (and variants) was assumed to follow a 1:1 binding model. As sensorgrams corresponding to multiple RBD concentrations were recorded, global fitting was performed for each temperature and variant. Both kinetic (k_{on} and k_{off}) and thermodynamic (K_D) constants were identified. The fits were performed via the Biacore Evaluation Software. To evaluate the appropriateness of the one-to-one binding assumption, a residual analysis was performed by comparing the recorded sensorgrams to the predicted sensorgrams calculated with the identified parameters. The standard deviation of the parameters obtained at different repetitions of the experiments were calculated to assess the repeatability of the SPR assay.

Van’t Hoff plots were used to determine the standard reaction enthalpy and entropy via their slope and intercept. They are based on the Van’t Hoff equation:

$$R_{IG}T\ln\left(K_D\right) = \Delta G^\circ = \Delta H^\circ - T\Delta S^\circ \quad (1)$$

$$\ln\left(K_D\right) = \frac{\Delta H^\circ}{R_{IG}T} - \frac{\Delta S^\circ}{R_{IG}}$$

R_{IG} denotes the ideal gas constant and T is the temperature. ΔG° is the Gibbs free energy of the pseudo-reaction, while ΔH° and ΔS° are the standard reaction enthalpy and the standard reaction entropy, respectively.

Data availability

The datasets generated during and/or analysed during the current study are available from the corresponding author on reasonable request.

Declarations

Data availability

The datasets generated during and/or analysed during the current study are available from the corresponding author on reasonable request.

Acknowledgement

This work was supported by the Pandemic Response Challenge Program of the National Research Council of Canada, the Natural Sciences and Engineering Research Council of Canada (stipend allocated to Catherine Forest-Nault and Jimmy Gaudreault via the NSERC-CREATE PrEEmiuM program) and the TransMedTech Institute (NanoBio Technology Platform) with its main funding partner, the Canada First Research Excellence Fund. The authors would also like to thank Benoit Liberelle, Romane Oliverio, Médéric Dégardin and Aymeric Guy for fruitful discussions during the writing of the manuscript and the display of results. This is NRC publication #NRCXXXXX.

Author information

Affiliation

Department of Chemical Engineering, Polytechnique Montreal, Montreal, Quebec, Canada, H3T 1J4

Catherine Forest-Nault, Jimmy Gaudreault, Gregory De Crescenzo and Olivier Henry

Human Health Therapeutics Research Centre, National Research Council of Canada, Montreal. Quebec, Canada, H4P 2R2

Izel Koyuturk, Alex Pelletier, Denis L'Abbé, Brian Cass, Louis Bisson, Alina Burlacu, Laurence Delafosse, Matthew Stuible and Yves Durocher

Department of Biochemistry and Molecular Medicine, University of Montreal; Montreal, Quebec, Canada, H3T 1J4

Yves Durocher and Izel Koyuturk

Corresponding author

Gregory De Crescenzo at gregory.decrescenzo@polymtl.ca

Contribution

Experiments and Analysis: C.F.N., I.K., J.G., M.S., L.D., L.B., D.L, A.P., B.C., and A.B.; Writing of the manuscript: C.F.N., I.K. Supervision, review and editing of the manuscript: G.D, Y.D. and O.H

Competing interests

The author(s) declare no competing interests.

References

1. WHO. Tracking SARS-CoV-2 variants. doi:https://www.who.int/en/activities/tracking-SARS-CoV-2-variants/ (2022).
2. Harvey, W. T. *et al.* SARS-CoV-2 variants, spike mutations and immune escape. Nature Reviews Microbiology **19**, 409–424, doi:10.1038/s41579-021-00573-0 (2021).
3. Wrapp, D. *et al.* Cryo-EM structure of the 2019-nCoV spike in the prefusion conformation. Science **367**, 1260–1263, doi:10.1126/science.abb2507 (2020).
4. Wang, Q. *et al.* Structural and Functional Basis of SARS-CoV-2 Entry by Using Human ACE2. *Cell* **181**, 894–904 e899, doi:10.1016/j.cell.2020.03.045 (2020).
5. Gan, H. H., Twaddle, A., Marchand, B. & Gunsalus, K. C. Structural Modeling of the SARS-CoV-2 Spike/Human ACE2 Complex Interface can Identify High-Affinity Variants Associated with Increased Transmissibility. Journal of Molecular Biology **433**, 167051, doi:https://doi.org/10.1016/j.jmb.2021.167051 (2021).
6. Deshpande, A., Harris, B. D., Martinez-Sobrido, L., Kobie, J. J. & Walter, M. R. Epitope Classification and RBD Binding Properties of Neutralizing Antibodies Against SARS-CoV-2 Variants of Concern. **12**, doi:10.3389/fimmu.2021.691715 (2021).
7. Barton, M. I. *et al.* Effects of common mutations in the SARS-CoV-2 Spike RBD and its ligand, the human ACE2 receptor on binding affinity and kinetics. eLife **10**, e70658, doi:10.7554/eLife.70658 (2021).
8. Raghu, D., Hamill, P., Banaji, A., McLaren, A. & Hsu, Y.-T. Assessment of the binding interactions of SARS-CoV-2 spike glycoprotein variants. Journal of Pharmaceutical Analysis,

doi:https://doi.org/10.1016/j.jpha.2021.09.006 (2021).

9. Laffeber, C., de Koning, K., Kanaar, R. & Lebbink, J. H. G. Experimental Evidence for Enhanced Receptor Binding by Rapidly Spreading SARS-CoV-2 Variants. Journal of molecular biology **433**, 167058–167058, doi:10.1016/j.jmb.2021.167058 (2021).
10. Supasa, P. *et al.* Reduced neutralization of SARS-CoV-2 B.1.1.7 variant by convalescent and vaccine sera. Cell **184**, 2201–2211.e2207, doi:10.1016/j.cell.2021.02.033 (2021).
11. Liu, H. *et al.* The basis of a more contagious 501Y.V1 variant of SARS-CoV-2. Cell Research **31**, 720–722, doi:10.1038/s41422-021-00496-8 (2021).
12. Shang, J. *et al.* Structural basis of receptor recognition by SARS-CoV-2. Nature **581**, 221–224, doi:10.1038/s41586-020-2179-y (2020).
13. Myszka, D. G. Improving biosensor analysis. Journal of Molecular Recognition **12**, 279–284, doi:https://doi.org/10.1002/(SICI)1099-1352(199909/10)12:5<279::AID-JMR473>3.0.CO;2-3 (1999).
14. Marquart, J. A. in *Handbook of Surface Plasmon Resonance (2)* 106–148 (The Royal Society of Chemistry, 2017).
15. Liu, H. *et al.* 501Y.V2 and 501Y.V3 variants of SARS-CoV-2 lose binding to bamlanivimab in vitro. mAbs **13**, 1919285, doi:10.1080/19420862.2021.1919285 (2021).
16. Lan, J. *et al.* Structure of the SARS-CoV-2 spike receptor-binding domain bound to the ACE2 receptor. Nature **581**, 215–220, doi:10.1038/s41586-020-2180-5 (2020).
17. Tian, F. *et al.* N501Y mutation of spike protein in SARS-CoV-2 strengthens its binding to receptor ACE2. *eLife* **10**, e69091, doi:10.7554/eLife.69091 (2021).
18. Murschel, F. *et al.* Coiled-coil-mediated grafting of bioactive vascular endothelial growth factor. Acta Biomaterialia **9**, 6806–6813, doi:https://doi.org/10.1016/j.actbio.2013.02.032 (2013).
19. De Crescenzo, G., Litowski, J. R., Hodges, R. S. & O'Connor-McCourt, M. D. Real-Time Monitoring of the Interactions of Two-Stranded de Novo Designed Coiled-Coils: Effect of Chain Length on the Kinetic and Thermodynamic Constants of Binding. Biochemistry **42**, 1754–1763, doi:10.1021/bi0268450 (2003).
20. Cambay, F., Henry, O., Durocher, Y. & De Crescenzo, G. Impact of N-glycosylation on Fcγ receptor / IgG interactions: unravelling differences with an enhanced surface plasmon resonance biosensor assay based on coiled-coil interactions. mAbs **11**, 435–452, doi:10.1080/19420862.2019.1581017 (2019).
21. Koyuturk, I. *et al.* High-level production of wild-type and oxidation-resistant recombinant alpha-1-2 antitrypsin in glycoengineered CHO cells *Biotechnology and Bioengineering* (2022).
22. Rich, R. L. & Myszka, D. G. Advances in surface plasmon resonance biosensor analysis. Current Opinion in Biotechnology **11**, 54–61, doi:https://doi.org/10.1016/S0958-1669(99)00054-3 (2000).
23. Crescenzo, G. D., Boucher, C., Durocher, Y. & Jolicoeur, M. Kinetic Characterization by Surface Plasmon Resonance-Based Biosensors: Principle and Emerging Trends. Cellular and Molecular Bioengineering **1**, 204–215, doi:10.1007/s12195-008-0035-5 (2008).

24. Kirchdoerfer, R. N. *et al.* Stabilized coronavirus spikes are resistant to conformational changes induced by receptor recognition or proteolysis. Scientific Reports **8**, 15701, doi:10.1038/s41598-018-34171-7 (2018).
25. Mannar, D. *et al.* SARS-CoV-2 Omicron variant: Antibody evasion and cryo-EM structure of spike protein–ACE2 complex. Science **375**, 760–764, doi:10.1126/science.abn7760 (2022).
26. Schuck, P. & Zhao, H. The role of mass transport limitation and surface heterogeneity in the biophysical characterization of macromolecular binding processes by SPR biosensing. Methods Mol Biol **627**, 15–54, doi:10.1007/978-1-60761-670-2_2 (2010).
27. Khalifa, M. B., Choulier, L., Lortat-Jacob, H., Altschuh, D. & Vernet, T. BIACORE Data Processing: An Evaluation of the Global Fitting Procedure. Analytical Biochemistry **293**, 194–203, doi:https://doi.org/10.1006/abio.2001.5119 (2001).
28. Van Der Merwe, P. A. J. P.-l. i. h. & calorimetry. Surface plasmon resonance. **1**, 137–170 (2001).
29. Forest-Nault, C., Gaudreault, J., Henry, O., Durocher, Y. & De Crescenzo, G. On the Use of Surface Plasmon Resonance Biosensing to Understand IgG-FcγR Interactions. International Journal of Molecular Sciences **22**, doi:10.3390/ijms22126616 (2021).
30. Ray, D., Le, L. & Andricioaei, I. Distant residues modulate conformational opening in SARS-CoV-2 spike protein. *Proceedings of the National Academy of Sciences* **118**, e2100943118, doi:10.1073/pnas.2100943118 (2021).
31. Zhao, X., Xiong, D., Luo, S. & Duan, L. Origin of the tight binding mode to ACE2 triggered by multi-point mutations in the omicron variant: a dynamic insight. Physical Chemistry Chemical Physics, doi:10.1039/D2CP00449F (2022).
32. Han, P. *et al.* Molecular insights into receptor binding of recent emerging SARS-CoV-2 variants. Nature Communications **12**, 6103, doi:10.1038/s41467-021-26401-w (2021).
33. Kim, S. *et al.* Differential Interactions between Human ACE2 and Spike RBD of SARS-CoV-2 Variants of Concern. J Chem Theory Comput **17**, 7972–7979, doi:10.1021/acs.jctc.1c00965 (2021).
34. Ali, F., Kasry, A. & Amin, M. The new SARS-CoV-2 strain shows a stronger binding affinity to ACE2 due to N501Y mutant. Medicine in Drug Discovery **10**, 100086, doi:https://doi.org/10.1016/j.medidd.2021.100086 (2021).
35. Han, P. *et al.* Receptor binding and complex structures of human ACE2 to spike RBD from omicron and delta SARS-CoV-2. Cell **185**, 630–640.
e610
, doi:https://doi.org/10.1016/j.cell.2022.01.001 (2022).
36. Liu, K. *et al.* Binding and molecular basis of the bat coronavirus RaTG13 virus to ACE2 in humans and other species. Cell **184**, 3438–3451.
e3410
, doi:https://doi.org/10.1016/j.cell.2021.05.031 (2021).
37. Zhang, Z. *et al.* The molecular basis for SARS-CoV-2 binding to dog ACE2. Nature Communications **12**, 4195, doi:10.1038/s41467-021-24326-y (2021).

38. Singh, A., Steinkellner, G., Köchl, K., Gruber, K. & Gruber, C. C. Serine 477 plays a crucial role in the interaction of the SARS-CoV-2 spike protein with the human receptor ACE2. Scientific Reports **11**, 4320, doi:10.1038/s41598-021-83761-5 (2021).
39. Cheng, M. H. *et al.* Impact of new variants on SARS-CoV-2 infectivity and neutralization: A molecular assessment of the alterations in the spike-host protein interactions. iScience **25**, 103939, doi:https://doi.org/10.1016/j.isci.2022.103939 (2022).
40. Chen, C. *et al.* Computational prediction of the effect of amino acid changes on the binding affinity between SARS-CoV-2 spike RBD and human ACE2. *Proceedings of the National Academy of Sciences* **118**, e2106480118, doi:10.1073/pnas.2106480118 (2021).
41. Thye, A. Y. *et al.* Emerging SARS-CoV-2 Variants of Concern (VOCs): An Impending Global Crisis. Biomedicines **9**, doi:10.3390/biomedicines9101303 (2021).
42. Liu, H., Wei, P., Kappler, J. W., Marrack, P. & Zhang, G. SARS-CoV-2 Variants of Concern and Variants of Interest Receptor Binding Domain Mutations and Virus Infectivity. **13**, doi:10.3389/fimmu.2022.825256 (2022).
43. Wang, Y. *et al.* Structural basis for SARS-CoV-2 Delta variant recognition of ACE2 receptor and broadly neutralizing antibodies. Nature Communications **13**, 871, doi:10.1038/s41467-022-28528-w (2022).
44. Ozono, S. *et al.* SARS-CoV-2 D614G spike mutation increases entry efficiency with enhanced ACE2-binding affinity. Nature Communications **12**, 848, doi:10.1038/s41467-021-21118-2 (2021).
45. Tchesnokova, V. *et al.* Acquisition of the L452R Mutation in the ACE2-Binding Interface of Spike Protein Triggers Recent Massive Expansion of SARS-CoV-2 Variants. Journal of Clinical Microbiology **59**, e00921-00921, doi:10.1128/JCM.00921-21.
46. Cherian, S. *et al.* SARS-CoV-2 Spike Mutations, L452R, T478K, E484Q and P681R, in the Second Wave of COVID-19 in Maharashtra, India. Microorganisms **9**, 1542, doi:10.3390/microorganisms9071542 (2021).
47. Motozono, C. *et al.* SARS-CoV-2 spike L452R variant evades cellular immunity and increases infectivity. Cell Host Microbe **29**, 1124–1136.e1111, doi:10.1016/j.chom.2021.06.006 (2021).
48. Cameroni, E. *et al.* Broadly neutralizing antibodies overcome SARS-CoV-2 Omicron antigenic shift. Nature **602**, 664–670, doi:10.1038/s41586-021-04386-2 (2022).
49. Xiong, D., Zhao, X., Luo, S. & Duan, L. Insights from computational analysis: how does the SARS-CoV-2 Delta (B.1.617.2) variant hijack ACE2 more effectively? Physical Chemistry Chemical Physics, doi:10.1039/D2CP00843B (2022).
50. Saville, J. W. *et al.* Structural and biochemical rationale for enhanced spike protein fitness in delta and kappa SARS-CoV-2 variants. Nature Communications **13**, 742, doi:10.1038/s41467-022-28324-6 (2022).
51. McCallum, M. *et al.* Molecular basis of immune evasion by the Delta and Kappa SARS-CoV-2 variants. Science **374**, 1621–1626, doi:10.1126/science.abl8506 (2021).

52. Goher, S. S., Ali, F. & Amin, M. The Delta Variant Mutations in the Receptor Binding Domain of SARS-CoV-2 Show Enhanced Electrostatic Interactions with the ACE2. Medicine in drug discovery, 100114–100114, doi:10.1016/j.medidd.2021.100114 (2021).
53. Cao, W. *et al.* Biomechanical characterization of SARS-CoV-2 spike RBD and human ACE2 protein-protein interaction. Biophys J **120**, 1011–1019, doi:10.1016/j.bpj.2021.02.007 (2021).
54. Mehdipour, A. R. & Hummer, G. Dual nature of human ACE2 glycosylation in binding to SARS-CoV-2 spike. Proc Natl Acad Sci U S A **118**, e2100425118, doi:10.1073/pnas.2100425118 (2021).
55. Allen, J. D., Watanabe, Y., Chawla, H., Newby, M. L. & Crispin, M. Subtle Influence of ACE2 Glycan Processing on SARS-CoV-2 Recognition. J Mol Biol **433**, 166762, doi:10.1016/j.jmb.2020.166762 (2021).
56. Nguyen, K., Chakraborty, S., Mansbach, R. A., Korber, B. & Gnanakaran, S. Exploring the Role of Glycans in the Interaction of SARS-CoV-2 RBD and Human Receptor ACE2. *Viruses* **13**, doi:10.3390/v13050927 (2021).
57. Bagdonaite, I. *et al.* Site-Specific O-Glycosylation Analysis of SARS-CoV-2 Spike Protein Produced in Insect and Human Cells. Viruses **13**, doi:10.3390/v13040551 (2021).
58. Shi, C. *et al.* Purification and Characterization of a Recombinant G-Protein-Coupled Receptor, Saccharomyces cerevisiae Ste2p, Transiently Expressed in HEK293 EBNA1 Cells. Biochemistry **44**, 15705–15714, doi:10.1021/bi051292p (2005).
59. Poulain, A., Mullick, A., Massie, B. & Durocher, Y. Reducing recombinant protein expression during CHO pool selection enhances frequency of high-producing cells. Journal of Biotechnology **296**, 32–41, doi:https://doi.org/10.1016/j.jbiotec.2019.03.009 (2019).
60. Stuible, M. *et al.* Rapid, high-yield production of full-length SARS-CoV-2 spike ectodomain by transient gene expression in CHO cells. Journal of Biotechnology **326**, 21–27, doi:https://doi.org/10.1016/j.jbiotec.2020.12.005 (2021).
61. Colwill, K. *et al.* A scalable serology solution for profiling humoral immune responses to SARS-CoV-2 infection and vaccination. Clinical & Translational Immunology **11**, e1380, doi:https://doi.org/10.1002/cti2.1380 (2022).
62. Litowski, J. R. & Hodges, R. S. Designing heterodimeric two-stranded α-helical coiled-coils: the effect of chain length on protein folding, stability and specificity. The Journal of Peptide Research **58**, 477–492, doi:https://doi.org/10.1034/j.1399-3011.2001.10972.x (2001).

Figures

Figure 1

Representation of our three-step SPR-based assay with capture of E5 coil tagged ACE2 (ACE2-E5) by a K5 coil surface

Figure 2

SPR sensorgrams recorded for the RBD variants that do not contain the L452R mutation interacting with tethered ACE2 at different temperatures. The sensorgrams corresponding to variant injections at 10, 25 and 37°C were globally fitted with a 1:1 Langmuir binding model (solid black lines). Residual plots are included underneath each sensorgram series.

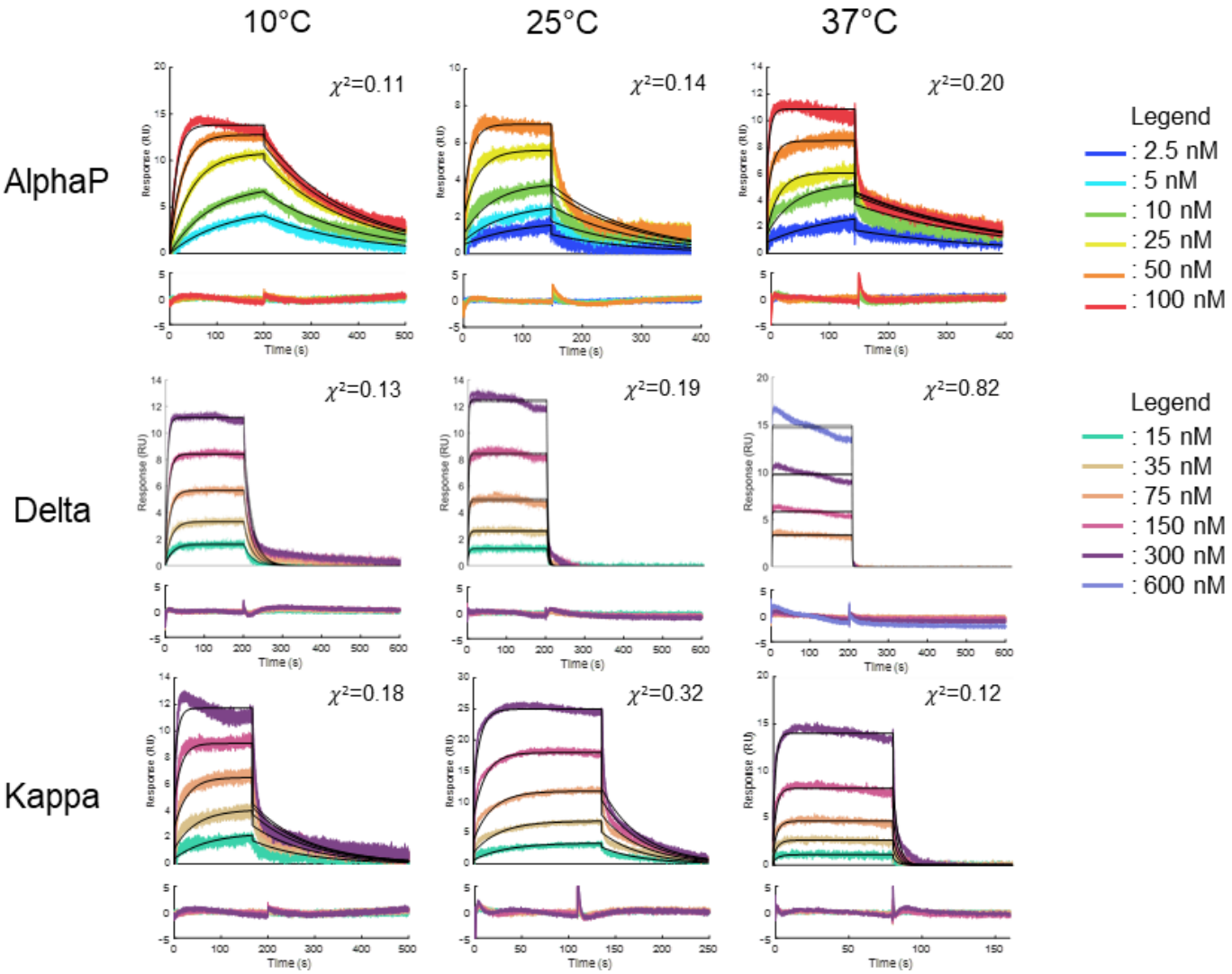

Figure 3

SPR sensorgrams recorded for the RBD variants with the L452R mutation interacting with tethered ACE2 at different temperatures. The sensorgrams corresponding to variant injections at 10, 25 and 37°C were globally fitted with a 1:1 Langmuir binding model (black solid lines). Residual plots are included underneath each sensorgram series

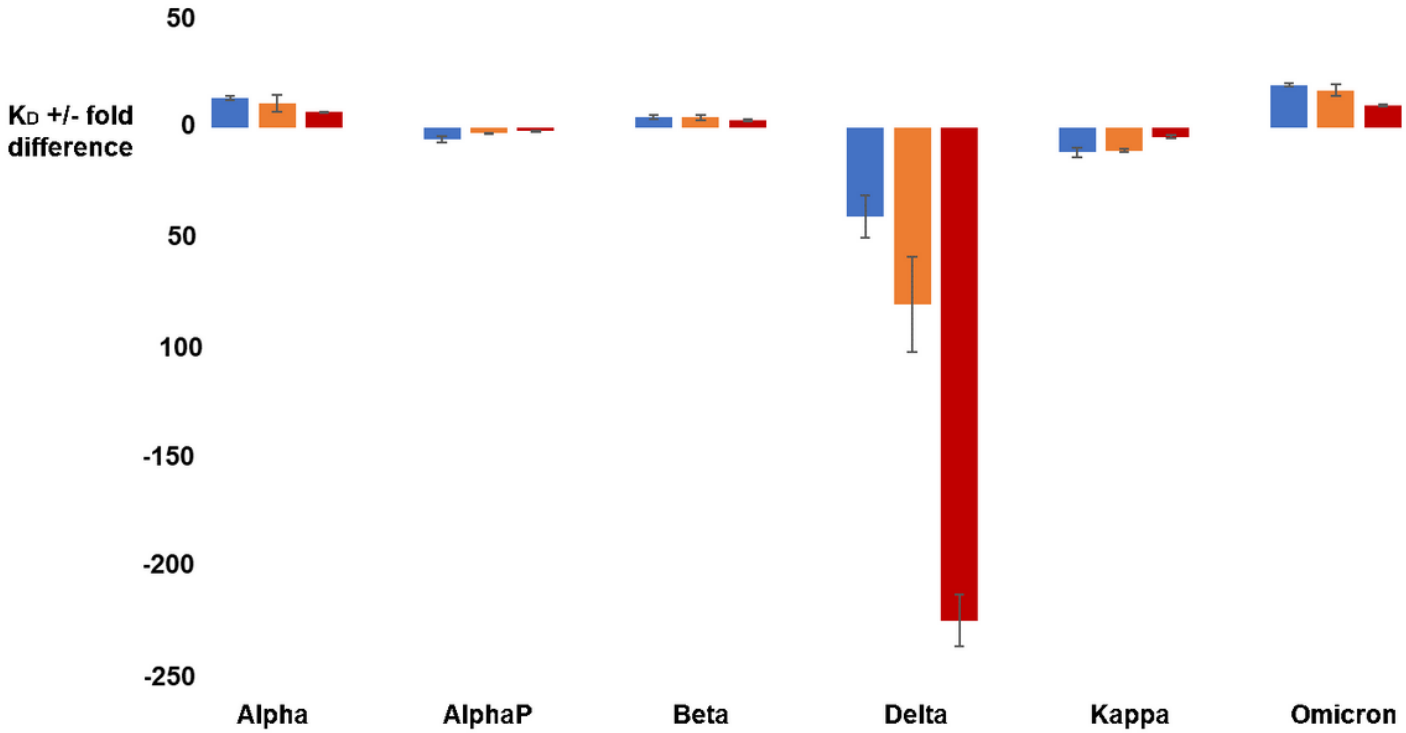

Figure 4

Comparison of the affinity of the RBD / ACE2 interaction at 10°C (in blue), 25°C (in orange) and 37°C (in red) for all RBD variants considered in this study. The fold difference with respect to the affinity of the wild type RBD at a given temperature is reported

Supplementary Files

This is a list of supplementary files associated with this preprint. Click to download.

- SupplementaryDataNaultetal.docx